How well does a Linear Static Finite Element Analysis Predict Measured Strains from a Nuclear Package Tie Down System during Rail Transportation?

Corresponding Author: Andrew Cummings †
Author: Dr. Glynn Rothwell ‡
Author: Dr. Christian Matthews ‡

†Corresponding author email address:
andrew.cummings@innuserv.com
International Nuclear Services
‡Liverpool John Moores University

Abstract

Freight rail is often the preferred method for transportation of dangerous goods. One particular application is the use of rail to convey radioactive material in purpose built packages. During transit, packages are secured to a rail wagon bed with a tie down system. The design of tie down systems vary considerably depending on package type and rail vehicle, for example shackles, turnbuckles, tie-rods, gravity wells or transport frames are all commonly used. There are also a large number of different packages in existence that all vary in size and mass; typically 1 - 7 m in length and 100 kg - 100 tonnes in mass. Despite the uniqueness of many transport configurations the design of tie down systems is always carried out using a limited set of design load cases as defined in the appropriate Codes of Practice and Standards. Many authors have suggested that the load cases within the standards need revision or question which load cases should apply to which scenario.
In a previous experiment accelerations and strains have been measured on a freight wagon and transport frame of a heavy package during a routine rail journey. From these data new insight into the magnitude and nature of loading has been gained. There is now, at least, limited supporting evidence of real world loading.
In the present study the measured accelerations have been used as input to a Finite Element Model (FEM) of the transport frame and a method based on correlation between predicted and measured strains has been developed to determine an appropriate low pass filter cutoff frequency, f_c, which separates quasi-static loading from raw dynamic data. The residual dynamic measurements have been assessed using signals processing techniques to understand their significance. The FEM has also been used to assess the presence of contact and boundary nonlinearities and how they affect the agreement between measured and predicted strains.

Keywords: Tie down system · package · acceleration · strain · rail

Introduction

The conventional safety record for transport of heavy packages by rail is very good with very few incidents or accidents reported. One important aspect of achieving and maintaining this level of safety is the thorough design of tie down systems. A broad spectrum of load cases due to the transportation environment are addressed during the development phase. Tie downs are required to withstand everyday operational usage including package loading/unloading, lifting, tilting and loads that arise during transportation. These requirements are satisfied by designing the system to possess sufficient strength.

The cyclic nature of the loads and the dynamic transportation loads require that the system also

possesses sufficient fatigue resistance. Additionally, in the event of an accident the tie down system must not damage the package in such a way that impairs its safety. This requirement has led to the design of weak links in some tie downs, ensuring that under a given accident condition the package safety is not compromised.

Cummings *et al* [1] described methods for filtering measured accelerations during a rail journey of a 99.7 tonne nuclear package. They estimated quasi-static accelerations for comparison with the current design parameters. In the present study dynamic acceleration and strain data is systematically passed through a low pass filter, whilst varying its cutoff frequency between 1 Hz - 100 Hz. The filtered tri-axial acceleration time histories are used to scale the results of a linear static Finite Element Model (FEM) at specific elements in the model corresponding to strain gauge locations. The scaled vertical, lateral and longitudinal accelerations are then summed to calculate strain time histories. The calculated strain time histories are compared with actual measurements.

A linear mathematical model has been used to predict the response of the tie down to the transportation loading. By studying correlation between measured and predicted strains it is possible to assess the limits of such a model and establish when the response of the tie-down is no longer linear. A successfully validated computer model has several key benefits:

1. Safety margins based on experimental results can be quantified.
2. Provides an opportunity to assess other areas of the structure where no measurements were taken.
3. Improves interpretation of experimental results i.e. provides a justification for choice of filter cutoff frequency (f_c) to obtain loads for design.
4. Presents the possibility of reconstructing acceleration time histories from the measured strains i.e. inversely determine tie down loading based on material response not structural motion.

A FEM of the tie down system has been constructed and its idealisation explained. Methods for simplifying the complex frame to package interface are emphasised. Linearisation of the interaction between contacting parts enables the scaling and superposition method used to calculate strain time histories. This requires careful analysis to determine the validity or error caused by omitting nonlinear effects.

Correlation between measured accelerations and strains

For linear static analysis to be applicable a linear dependency between the measured accelerations and strains must exist. If the strains are linearly dependent on the accelerations then, in theory, they can be predicted using a suitable mathematical model which relates them.

The Pearson correlation coefficient (ρ) is calculated as follows:-

$$\rho = \frac{C_{xy}}{\sigma_x \sigma_y}$$

where:-

C_{xy} = Covariance between two random variables x and y

σ_x = Standard deviation of x

σ_y = Standard deviation of y

The correlation coefficient provides a measure of linear dependency between two sets of random data [2]. When comparing acceleration and strain signals $\rho = \pm 1$ for perfect linear dependency and $\rho = 0$ when the strains and accelerations are independent of each other.

Assessing the Strength of the Correlation

Wirsching *et al* [2] provide guidance on intepreting intermediate values of ρ however it is useful to first highlight some of the sources of random error or noise that weaken correlation. In signals analysis the terminology strength or weakness indicate the degree of dependance between one signal and another. Three main sources of error are proposed in **Figure 1**.

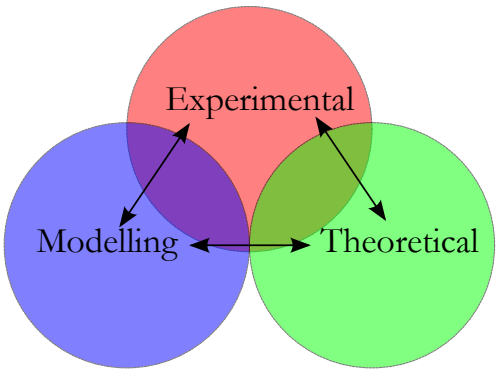

Figure 1: Sources of Error

When ρ deviates from ± 1 at least one or more of these sources are the cause of the weakened correlation. The total error can be described as follows:-

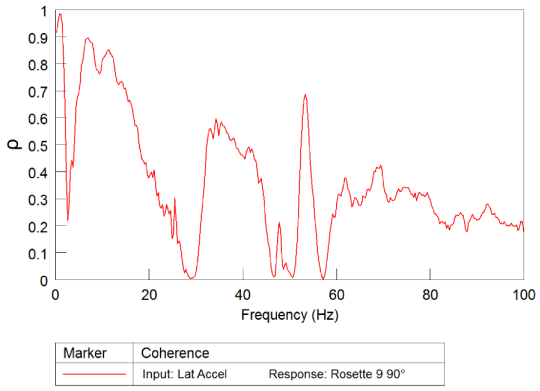

(a) 0 - 100 Hz

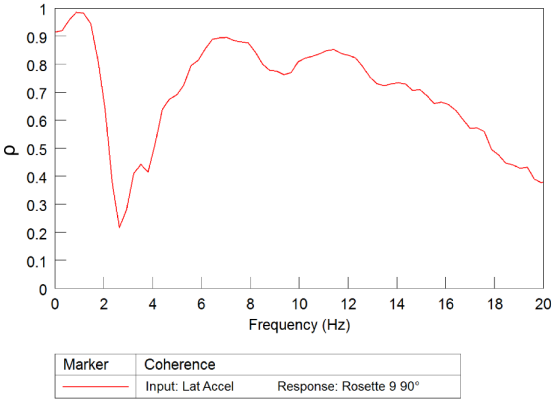

(b) 0 - 20 Hz

Figure 2: Example of Coherence between Measured Acceleration and Strain

$$\epsilon_{total} =$$
$$\epsilon_{experimental} + \epsilon_{modelling} + \epsilon_{theoretical}$$

Breaking down these sources of error further, to pinpoint root causes of weak correlation:-

$$\epsilon_{experimental} =$$
$$\epsilon_{electrical} + \epsilon_{temperature} + \epsilon_{procedural}$$
$$\epsilon_{modelling} =$$
$$\epsilon_{modelling\ assumptions} + \epsilon_{numerical\ (rounding)}$$
$$\epsilon_{theoretical} =$$
$$\epsilon_{nonlinearities} + \epsilon_{dynamic\ effects}$$

Each of these error sources consist of a number of different variables that degrade the strength of the correlation. Wirsching [2] suggests that if the total random error is $1/2$ the strength of the signal then $\rho \approx 0.9$ and the dependency between the signals is considered strong.

If the error is about the same strength as the signal then $\rho \approx 0.7$ and the dependency between the signals is considered moderate. An indication of weak dependence of strains on accelerations is $\rho < 0.7$.

The Coherence function calculates the correlation coefficient across a range of frequencies for a given input and output time history or channel. Based on an examination of the magnitude and direction of each strain channel it was evident that the strain response was dominated by lateral loading. Therefore the coherence function for each strain channel was calculated using the lateral acceleration measurements from the tie down system base end stanchion as the input channel. **Figure 2a** shows an example of a coherence function with the frequency axis set to 0 - 100 Hz.

Figure 2b shows the same coherence plot between 0 - 20 Hz. This frequency range has been chosen because the anticipated quasi-static content of the signal is < 20 Hz. The coherence function shows that all the signals are at least moderately correlated between 0 - 2 Hz and 5 - 15 Hz. This suggests that a linear model is appropriate, at least for this frequency range.

This simple coherance analysis treats the tie-down as a single input, single output system, however in reality there are multiple inputs that influence the output. Therefore, the combination of multi-axial accelerations, should increase the coherance in the 2 - 5 Hz range.

Data Cleansing

Data cleansing is a necessary process to make a comparison between calculated and measured peak strains. It is common practice to carry out some basic data cleansing normally to remove any DC offset and very low frequency content (drift) [3, 4].

The acceleration data was visually examined and not corrected further. However it was observed that the strains were very low, close to the noisefloor of the instrumentation in some cases. Because of this any small amount of drift and offset that is present is evident visually.

The drift present may be due to real physical loading such as thermal expansion. It may also be attributed to thermal errors, however this was minimised by the use of temperature compensated strain gauges [3]. Where necessary an attempt to remove drift was made using 1st or 2nd order polynomial curves (**Figure 3**). The removal of drift does not affect correlation, it just allows better comparison of peaks.

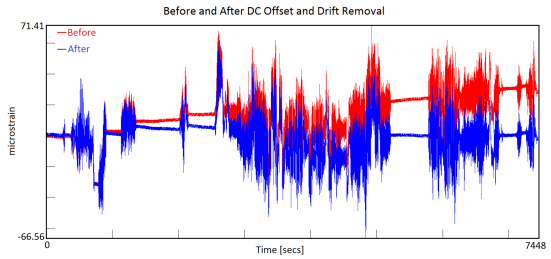

Figure 3: An Example of Data Cleansing used on some of the Measured Strain Time Histories

Tie Down System - General Arrangement

Figure 4 shows an exploded 3-D CAD model of the tie down system (inset is the assembled structure). The main structural members are the saddles, longitudinal beams and stanchions, all manufactured from high strength stainless steel plates and joined by welding. The trunnion bushes are made of a phosphur bronze (**Figure 5**).

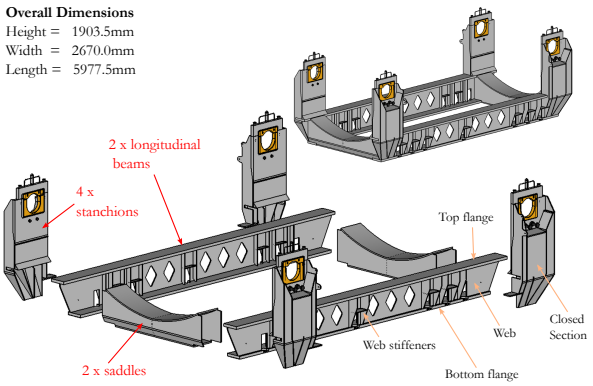

Figure 4: Details of the Tie Down System Construction

A mixture of partial and full penetration butt welds are used for joining the plates. Where possible the welds are double sided, however many closed sections exist and the welds are often, by necessity, single sided. Additionally due to its large size the welds are all manual and therefore stop/start sections are expected.

Figure 5 shows a close up of the package trunnion interface at the lid end stanchion of the tie down system. The trunnion bush is designed to allow ±20 mm of longitudinal sliding due to package thermal expansion/contraction. This is an area of analytical complexity for two reasons. The first is that this area consists of many contacting parts (some omitted here for clarity). The second is the geometrical configuration of the stanchion which enforces modelling simplifications, often in areas that warrant detail.

For example the backing plate (**Figure 5**) is a compound section, consisting of a 50 mm thick section at the trunnion bushes, a tapered section and 15 mm thick section at its base. The lateral restraint bolts combined with the irregular welded structure on the backing plate outward facing surface and the keep plates and their bolts are difficult to mesh with brick elements, but not suitable for shell element idealisation, therefore some modelling compromises are necessary.

The overarching compromise arises when connecting a hybrid shell and brick element mesh together. There is a disparity in nodal degrees of freedom between the two element types and the usual method of eliminating unwanted mechanisms due to this is by adding an extra row of shell elements "painted" over the surface of the connecting bricks. This method approximates load transfer across the joints but predicted stresses and strains at this type of interface are often in doubt.

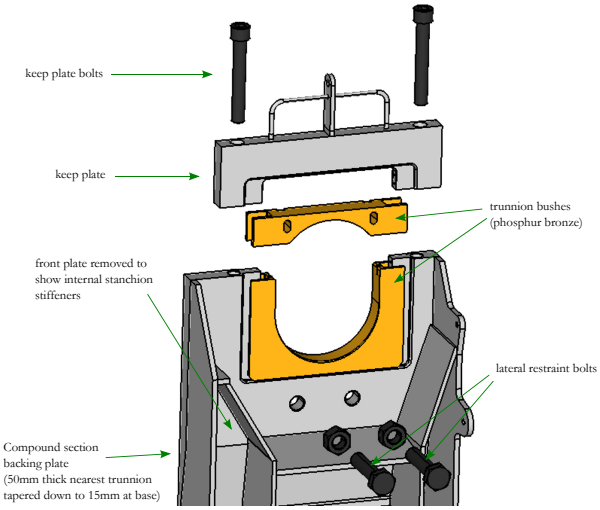

Figure 5: Detail of Lid End Trunnion Bushes and Upper Stanchion

Finite Element Model

The model was pre-processed using Hyperworks 12.0 [5]. All solutions were obtained using the sparse, direct, linear solver in Abaqus 6.13 [6]. **Figure 6** shows a wireframe view of the entire tie down system and a dummy package. As only limited information on the package was available it was modelled, excluding shock absorbers, with 4-noded tetrahedral elements and the density of the linear elastic material model was adjusted to obtain a mass of 99.7 tonnes.

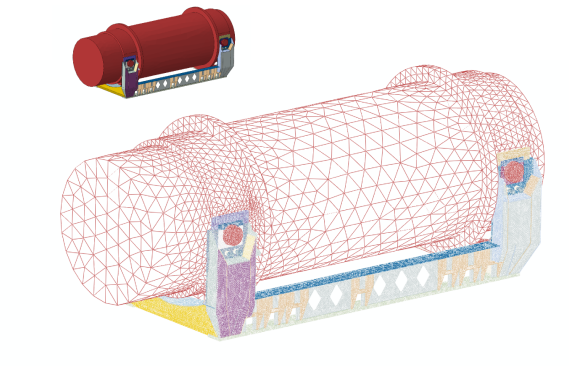

Figure 6: Finite Element Model of Tie Down System and Dummy Package

Details of the finite element mesh of the tie down are shown in **Figure 7**. The mesh consists of a mixture of 8-node brick elements and 4-node shell elements (C3D8 and S4). To maintain good element shape a small number of wedge and triangular elements have been used. A total of 568,416 elements: 135,696 quadrilaterals, 108 triangles, 394,340 bricks and 258 wedges were used in the model.

A global element size of 15 mm was selected, although smaller elements were used in some areas to resolve intricate details properly.

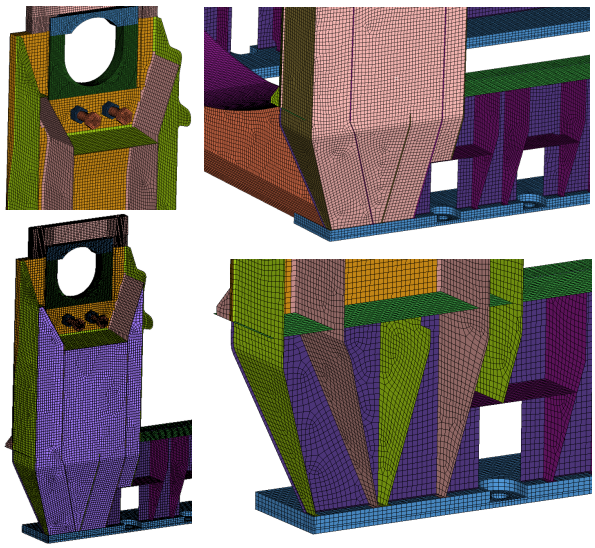

Figure 7: Details of Finite Element Mesh of Tie Down System

The mesh of the trunnion interface has retained most of the original design detail however the keep plate bolts and wear plates beneath the sliding lid end trunnion bush have been omitted. The interacting parts have been meshed with a finer, solid element mesh (≈5 mm) this allows obvious definition of master and slave surfaces in nonlinear sensitivity studies. Included in the model are the lateral restraint bolts represented with solid elements; their threaded portions are modelled by merging the nodes at the interface between the bolts, nuts and the stanchion back plates. **Figure 8** shows the mesh of the lid end trunnion attachments and lateral restraint bolts.

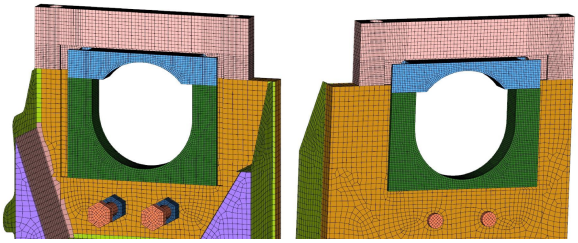

Figure 8: Finite Element Mesh of Lid End Trunnion Attachments and Restraint Bolts

Materials Modelling

During the rail journey the tie down system was not subjected to loads sufficient to cause nonlinear material behaviour. Therefore in this model all the materials have been modelled with a linear elastic material model, the properties used are listed in **Table 1** and the 0.2% yield stress is provided for reference.

Boundary Conditions and Loads

The package is mounted to the tie down system which is bolted to the rail wagon (**Figure 9**). The configuration of the rail wagon is an 8-axle wagon with four bogies connected to two sub frames with centre bowls and sidebearers. The subframes are connected to the superstructure with a centre pivot and sidebearers.

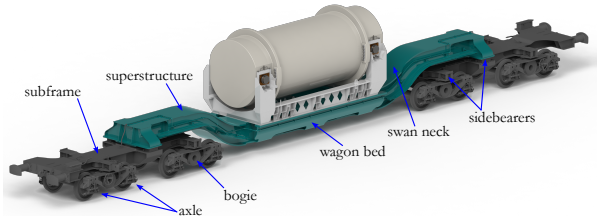

Figure 9: Major Components and Features of the Rail Wagon

The tie down system is connected to the swan neck wagon bed with 14 x M45 bolts. To isolate the tie down from the wagon it is necessary to constrain the model to eliminate any rigid body motion. In this analysis the tie down bolts are omitted and the entire lower surface of the bottom flange of the longitudinal beams is constrained (**Figure 10**). This overconstrains the

Material	Grade	ρ $[kg/m^3]$	E [GPa]	ν	$\sigma_{0.2\%}$ [MPa]	References
High Strength Stainless Steel	S890Q	7,800	200	0.3	960	[7]
Phosphur Bronze		7,600	121	0.3	123	[8]
Carbon Bolt Steel	BS898 12.9	7,800	192	0.3	1100	[9]

Table 1: Material Properties applied to Finite Element Model

structure slightly but sensitivity analysis showed that alternative methods, such as constraining only the nodes at the bolt holes, produced minor differences in structural response.

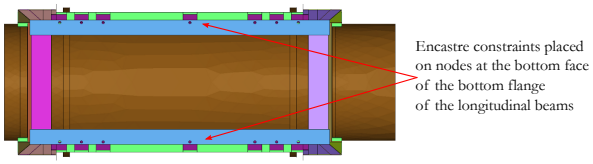

Figure 10: Boundary Conditions Applied to the Model

The unit load model was run in three uncoupled, linear perturbation steps, with a different load cases for each step (**Figure 11**). Distributed loads were used to apply an acceleration of 1 g to the whole model in the lateral, longitudinal and vertical directions. A comparison of the total computation time for the model is shown for 1, 2, 4, 6 and 8 CPUs (**Table 2**).

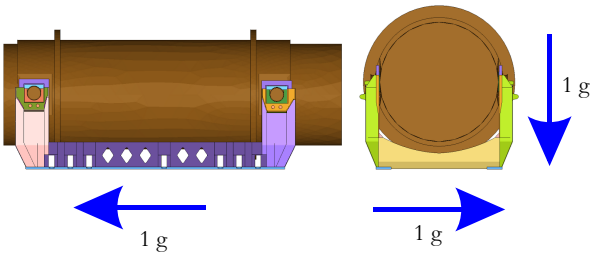

Figure 11: 3 x 1g Load Cases (Unit Loads)

CPUs	Wall Clock Time [min:secs]	RAM [Gbytes]
1	11:30	13
2	10: 5	13
4	9:28	13
6	8:47	13
8	8:48	13

Table 2: Run Times to Completion for Linear Model

Calculating Strain Time Histories

To obtain strain time histories a combination of scaling and superposition of the FEA results was used with the measured acceleration time histories as follows [10, 11]:-

$$\varepsilon_{ij}(t) = \sum_{k=1}^{N} \varepsilon_{(ij,k)} L_k(t)$$

$\varepsilon_{ij}(t)$ = the strain tensor at a time t

$\varepsilon_{ij,k}$ = the strain tensor due to unit load

$L_k(t)$ = the acceleration time history

where

k = lateral, vertical or longitudinal loading

Elements were selected that correspond to the measured strain locations and their strain tensors used in the scaling and superposition algorithm (**Figure 12**). This method accounts for multi-axial loading of the structure. A 30-minute section of the measurements during the journey were low pass filtered with a 4th order, forward-backward, Butterworth filter. Strain time histories were calculated using the filtered accelerations measured at the base end stanchion. This process was repeated for 28 different filter cut-off frequencies 1 Hz - 20 Hz in 1 Hz increments and 20 Hz - 100 Hz in 10 Hz increments. These calculations were carried out in nCode DesignLife [12].

Contact Modelling

Modelling the contacting parts has been achieved by either, meshing parts congruently and merging the nodes at the mating interfaces or by modelling with a contact pair, which is then tied, effectively bonding the parts together and achieving the desired linearisation.

Both methods require several important assumptions to hold or they will produce inaccurate results due to load path variations caused by sliding between contacting surfaces. Sensitivity

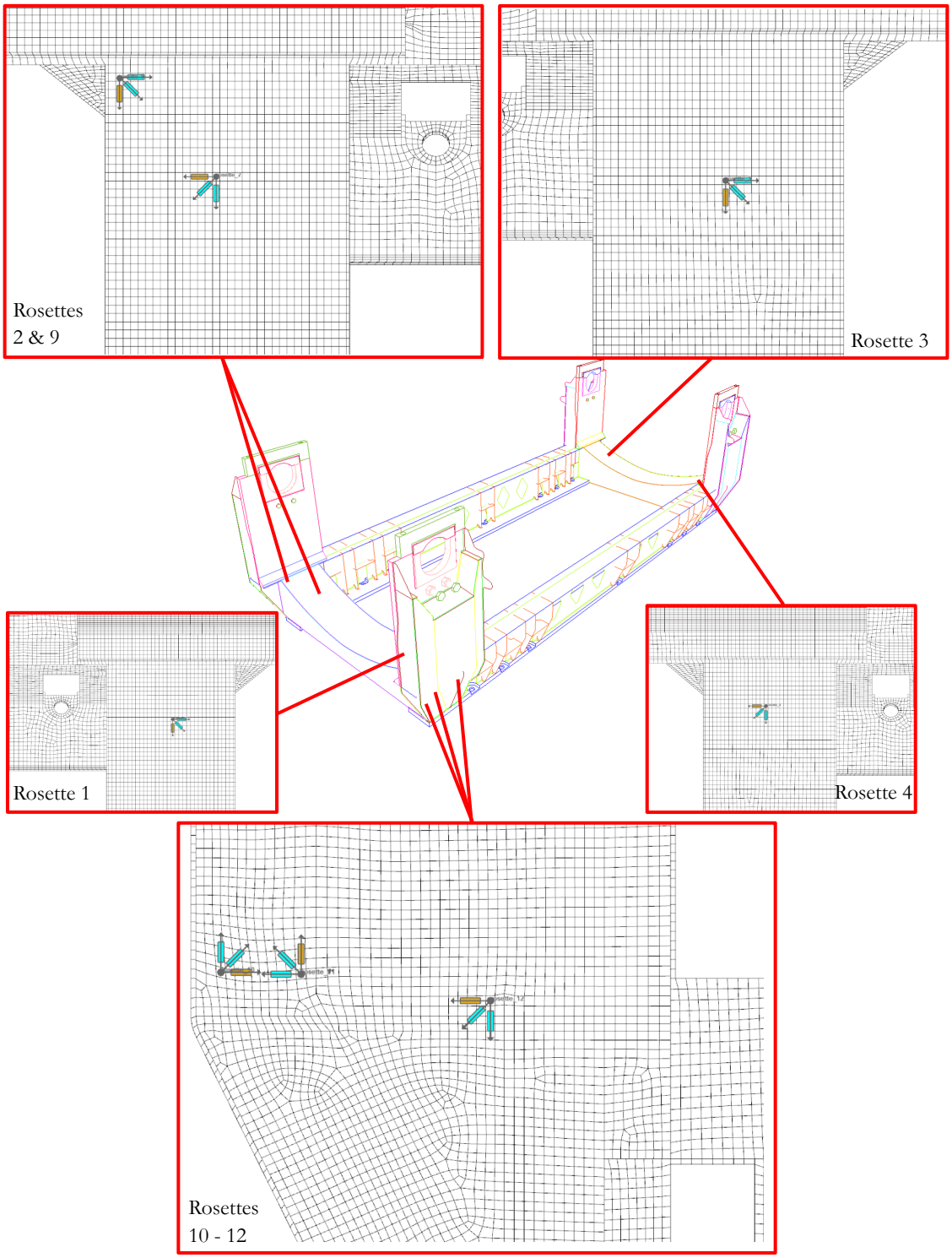

Figure 12: Locations and Orientations of the Virtual Strain Gauges

analysis has been carried out to confirm the validity and effect of the major assumptions. There is a lot of contact present between the parts of the tie down system, rail wagon and package; the two most important contact interactions for this study are now identified and discussed.

Contact at the Trunnion Attachments

There are several contacting parts in the trunnion attachments of the tie down system (**Figure 5**). The floating lid end trunnion bush could cause sliding and nonlinear geometric effects which may affect the strain results in the stanchions. A hand calculation, assuming a coefficient of friction μ =

0.35 which is typical of steel to phosphur bronze contact, shows that an acceleration of 0.1 g would be enough to overcome friction, resulting in sliding of the trunnion bush. This could arise due to heavy braking or cornering at speed. Lateral sliding of the trunnion bush is prevented due to the lateral restraint bolts, however only frictional forces prevent the floating trunnion bush from sliding due to longitudinal loading.

Lateral Restraint Bolts

The lateral restraint bolts are fitted to the tie down system through threaded holes in the stanchion back plates. They are adjusted to make contact with the package prior to transportation and held in place with a locking nut. This will produce a small bearing stress between the package side wall and the end of the bolt shank. Under lateral loading a change in the load paths may occur, as one stanchion will bend away from the restraint bolts, causing them to experience a compressive force exerted by the package and transmitted through to the stanchion. The opposite stanchion will bend towards the package, therefore any bearing stress between the end of the restraint bolt and the package side wall will decrease or in the limiting case, contact will be lost, resulting in differences in stanchion stresses and strains under reversed loading.

Sensitivity Analysis

A preliminary review of the modelling assumptions and loading was carried out to assess the validity of the scaling and superposition approach. Low pass filtering of measured accelerations with a cutoff frequency of 20 Hz produced the following load ranges:-

Lateral = [-0.16g, 0.16g]
Longitudinal = [-0.11g, 0.09g]
Vertical = [-0.26g, 0.22g] (excluding gravity)

Accelerations in the frequency range 0 - 100Hz, produced larger load ranges:-

Lateral = [-0.18g, 0.23g]
Longitudinal = [-0.32g, 0.12g]
Vertical = [-0.32g, 0.26g] (excluding gravity)

In the frequency range 0 - 100 Hz the longitudinal accelerations are large enough to cause sliding of the trunnion bushes. In this paper it is postulated that these peak accelerations occur too rapidly to introduce noticeable nonlinearity in the response of the tie-down system. The lateral and vertical load ranges do not vary significantly with f_c, however, the lateral loading may be enough to cause contact loss between the package and restraint bolts.

In the following section FEA results are compared by reviewing stresses at elements corresponding to the strain gauge positions. These elements are called the virtual strain gauge rosettes (**Figure 12**).

Nonlinear Effects during Longitudinal Loading

To assess the effects of using a tied contact at the "floating" lid end trunnion bushes, a half symmetry model was created for nonlinear analysis. The symmetry model retained five of the virtual strain gauge rosettes. The package was remodelled in brick elements with a refined mesh at the lateral restraint bolt contact areas and the trunnions (**Figure 13**).

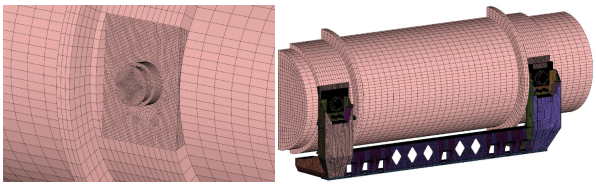

Figure 13: Detailed Mesh of Package Required for Nonlinear Studies

Speckert published a method for calculating time histories on a rail vehicle ball joint based on a set of nonlinear analyses that represent various combinations of load direction and magnitude [13]. Here a nonlinear analysis has been carried out to assess the contact effects of the trunnion bushes and lateral restraint bolts on the FEA results.

The analysis is run in two sequential load steps; the first to calculate a vertical preload due to gravity and also include the range of vertical loading. In the second step, a range of longitudinal loads have been prescribed, a matrix of runs is provided in **Table 3**. Consideration of the combined vertical and longitudinal load cases is necessary to obtain contact forces between the trunnion bushes, tie down and package that resist longitudinal motion.

The half symmetry model consisted of 414,535 elements and produced 1.7×10^6 degrees of freedom. A single model ran in approximately 1.5 hours on 8 CPUs and used 23 gigabytes of RAM. The 30 nonlinear runs were solved on a Linux server.

To reduce the overall solution time the first step was run only once per vertical load and a

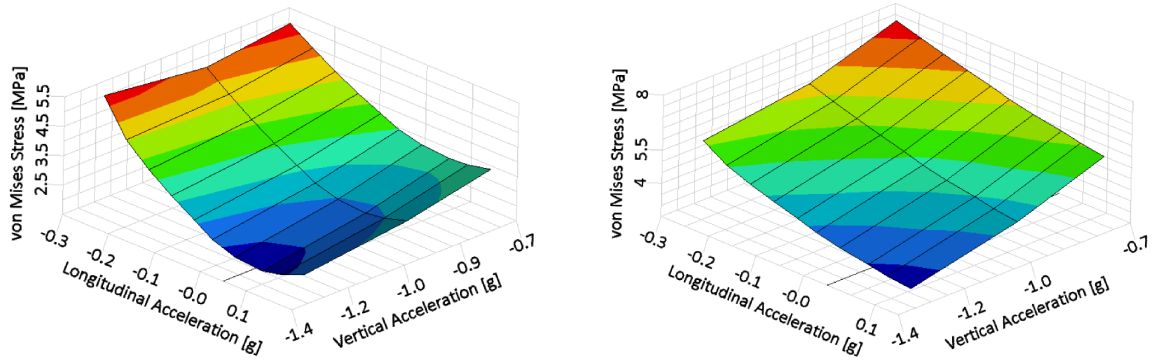

(a) Rosette 10 **(b) Rosette 12**

Figure 14: Example of von Mises Stress Results from Virtual Strain Gauges during Combined Longitudinal and Vertical Loading

Load Cases - Longitudinal Acceleration [g]										
Vertical	**Longitudinal**									
-1.32	-0.32	-0.27	-0.22	-0.17	-0.12	-0.07	-0.03	0.03	0.07	0.12
-1.0	-0.32	-0.27	-0.22	-0.17	-0.12	-0.07	-0.03	0.03	0.07	0.12
-0.74	-0.32	-0.27	-0.22	-0.17	-0.12	-0.07	-0.03	0.03	0.07	0.12

Table 3: Combination of Loading in Nonlinear Analysis

restarted analysis was then used to vary the longitudinal load cases. The line search method was used which provided additional computational efficiency. These techniques reduced the overall computation time from (an estimated) two days to approximately 5 hours. Both the pre and post processing were automated with a combination of shell scripts and HyperMath programming [5].

Figure 14 shows that the von Mises stress response is nonlinear in the load space analysed (i.e. lateral acceleration set to zero). The predicted stresses are very low for all five of the virtual rosettes, which is in agreement with the strain measurements that did not appear to be influenced by longitudinal loading. The Finite Element results do demonstrate that nonlinearity is present and significant in this tie-down system, however it will have a diminishingly small effect on this study because of the negligible influence of longitudinal loading during the experiment.

Nonlinear Effects during Lateral Loading

The half symmetry tie-down model and remodelled package were reflected and combined by merging the nodes on the symmetry plane to produce a complete FEA model for nonlinear analysis of lateral loading. The potential for nonlinear effects arising during lateral loading was considered to be independent of the other loading directions. This is because the contact pressure that develops between the lateral restraint bolts and the package side wall is not due to gravitational effects. This analysis was also carried out in two steps. Gravity was applied in the first step, to make the stresses comparable to the nonlinear longitudinal study and the results of this step were restarted for 10 lateral load cases in the range -0.23 g to 0.18 g.

Figure 15 provides a schematic to show the effects of the lateral restraint bolts contacting the package side wall during lateral loading. It is clear that the effective bending moment arm changes during load reversals, something that the linearised unit load model cannot account for.

At all the virtual strain gauges the von Mises stresses due to lateral loading are much larger than those predicted due to longitudinal loading.

The virtual strain gauges 10 - 12 are most likely to be effected by the bending response of the stanchion due to the presence of contact nonlinearity. (**Figure 16**) presents the results from rosette 10 and 12 for both the non-linear and unit load analyses.

The stress results called *"Nonlinear contact opening"* are due to positive lateral loads which cause the contact between the trunnnion restraint bolts and package to open. Those called *"Nonlinear contact closed"* are due to negative lateral loads (or a reversal) that causes the gap between the trunnion restraint bolts and the package to close and contact pressure to develop. The unit load model results are called *Linear bonded*, the

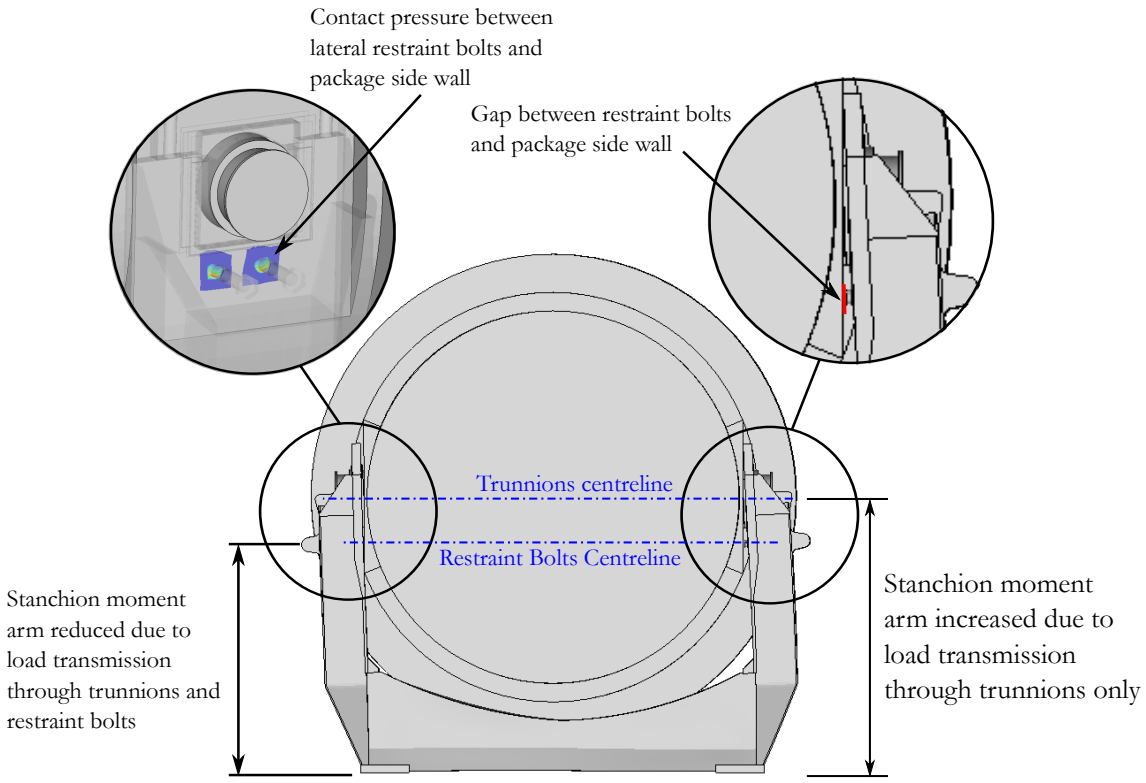

Figure 15: Sensitivity Analysis, Non-Linear Lateral Load Case to Assess the Effects of Discontinuous Contact Behaviour between the Package Side Walls and Tie-Down Lateral Restraint Bolts

lateral restraint bolts are effectively glued to the side wall of the package.

The results are fitted with trend lines and their coefficient of determination is annotated. This provides a measure of how linear the stress response is to increased loading.

The R^2 values are all very close to 1, confirming the applicability of scaling the linear lateral results. Also the stresses due to the nonlinear load reversals tend to bound those from the linear model. The difference in all the stress results was small, so the unit load model was considered a suitable candidate for comparison with the experiment.

Vertical Load Application

The presence of gravity causes the load range to be offset by -1 g. When applying the unit load this has been neglected because during the experimental procedure the strains and accelerations were measured during the loading of the package onto the tie down system and then zeroed prior to the journey. Therefore both positive and negative, measured vertical accelerations and tensile and compressive measured strains result from vertical loading.

The tensile strains due to vertical loading are offset by the compressive preload on the structure due to gravity. In reality the strains resulting from vertical loading will remain compressive unless a vertical acceleration > 1 g is experienced. If this does occur then the package is essentially weightless and the load path changes significantly. In this case the unit load model will not predict the load reversal correctly, however in the experiment the largest upwards, vertical acceleration was 0.26 g.

The direction of load applied to the model is also important as it changes the sign of the predicted stresses. It was necessary to account for this in the superposition procedure by premultiplying the acceleration time history by -1.0.

Correlation between Predicted and Measured Strains

For a quantitative assessment of the correlation between the measured and calculated strain time histories a script was written to calculate the correlation coefficient for each of the signals generated at different filter cutoff frequencies in HyperMath. The results are plotted as correlation coefficient vs filter cutoff frequency for each of the strain gauge rosettes (**Figure 17**).

It is evident that a number of the channels pro-

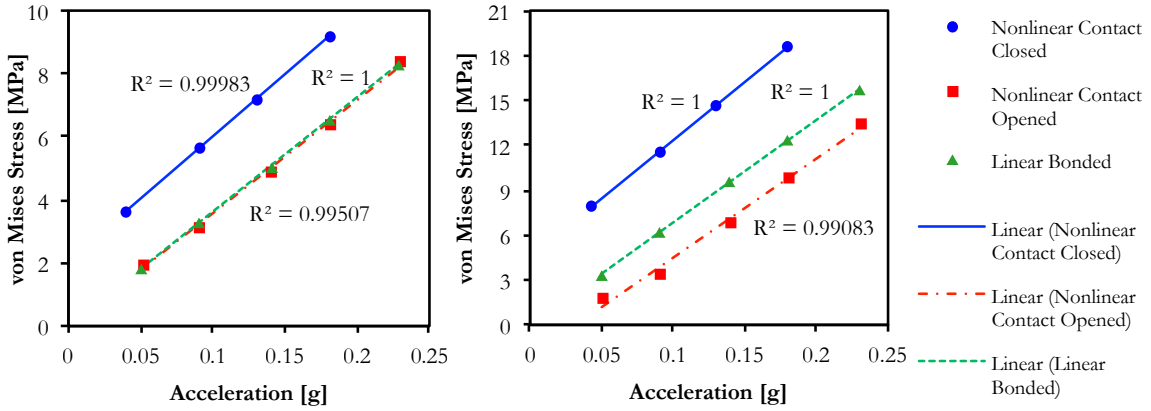

a. Rosette 10 **b. Rosette 12**

Figure 16: Sensitivity Analysis, Example of Nonlinear and Linear Load Case Stress Results from two Virtual Strain Gauges and a Linear Curve Fitting Trend Analysis which demonstrates the Linear Relationship between Increasing Lateral Load and Stress Response

duced poor agreement particularly at frequencies > 5 Hz. Visual examination of the signals with weak correlation indicated that some of the channels contained strain content $< \pm 10$ μmm/mm. These channels were discarded from any further processing because they were considered small enough to be structurally insignificant and also too low to be accurately represented by the finite element model. The remaining results were collated and are shown in **Figure 18**.

At filter cutoff frequencies < 5 Hz all the channels achieve at least moderate correlation ($\rho > 0.7$) and in many cases strong correlation ($\rho > 0.9$). **Figure 18** shows that there are 2 channels that still produce very weak correlation > 5 Hz. The anomalous results were found on two legs of rosette 3 (the third leg was previously discarded due to low strains levels). This was the only rosette, in the collated results, that was situated at the lid end of the structure. Therefore rosette 3 was re-run using the acceleration time histories from a lid end accelerometer. This was the subject of further investigation discussed later. The final correlation results are shown in **Figure 19**.

Five of the eight channels display strong correlation between 2 Hz - 5 Hz. At frequencies above 5 Hz the correlation is moderate and constant between 10 - 20 Hz, $\rho \approx 0.8$. As the f_c increases above 20 Hz the correlation becomes weaker.

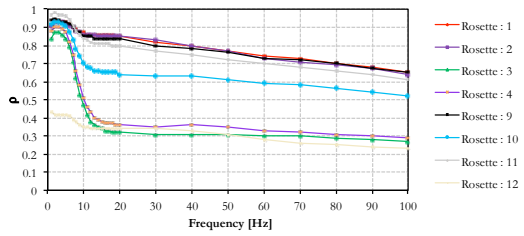

(a) Strain Gauge Correlation (0°leg of rosette)

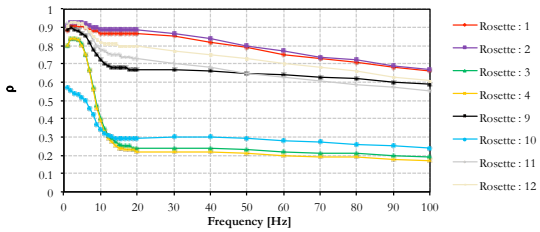

(b) Strain Gauge Correlation (45°leg of rosette)

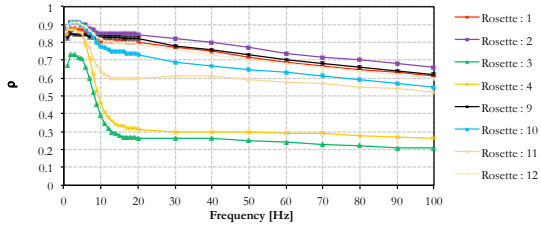

(c) Strain Gauge Correlation (90°leg of rosette)

Figure 17: Preliminary Correlation Results

Due to the large size of each time history, which contained 2 x 10^6 points, smooth scatter cross plots and time history slices have been used to provide a visual indication of the correlation (**Figure 20**) [14]. Rosette 12 was selected for use in **Figure 20** because it provided a typical ex-

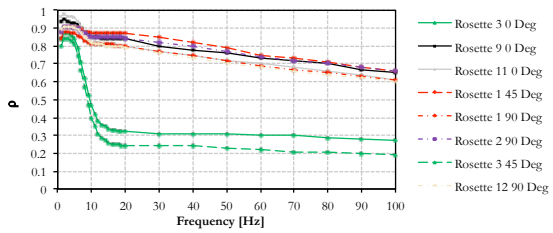

Figure 18: Correlation Results with Channels < 10 μmm/mm Removed

ample consistent with the results from the other virtual strain gauges. The most extreme outliers in the data are shown in the cross plots as small black points and a smoothing contour kernel used to blend the colours to distinguish densely populated areas of the cross plot from sparsely populated areas. The colour blue indicates the highest density of points and as the density decreases blue changes to red and then from red to white. The results indicate that as the f_c is reduced the outliers become more clustered and the scatter reduces.

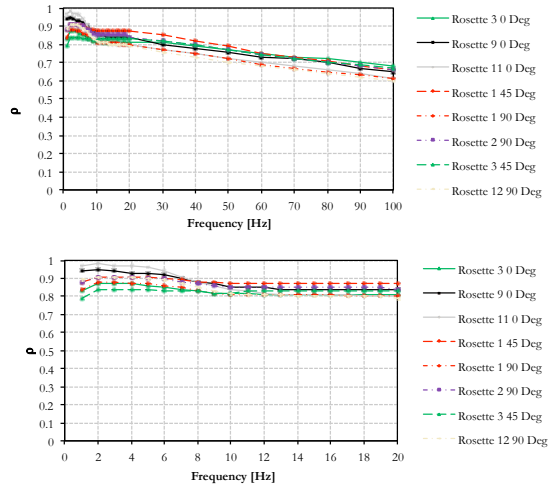

Figure 19: Final Correlation Results

The time history slices were produced by setting a time window that displayed approximately 10 cycles based on the f_c. Several different starting points were analysed, here an example is shown at 280 seconds that illustrates the effects of the filters in the time domain. The weak correlation obtained with $f_c = 100$ Hz is characterised by small high frequency oscillations in the FEA strains which arise due to the noisy acceleration measurements at high frequency.

The weakest correlation was found on rosette 12, filtered at 100 Hz, $\rho = 0.6$ (**Figures 20a & 20b**). Moderate correlation was achieved on rosette 12, filtered at 20 Hz, $\rho = 0.79$ (**Figures 20c & 20d**). Very strong correlation was achieved on rosette 12, filtered at 2 Hz, $\rho = 0.91$ (**Figures 20e & 20f**). The strongest correlation achieved was $\rho = 0.98$ on Rosette 11.

Analysis of Residuals

The residuals between the correlated and measured time histories have been compared using spectral analysis and autocorrelation functions. All computations were carried out using the open source, high level interpreted language GNU Octave and verified with the commercial software nCode Glyphworks [12, 15].

Initially the PSDs of the measured and predicted signals where overlaid. This pinpoints which frequencies match between experiment and analysis. To quantify the level of agreement the residuals were calculated by subtracting corresponding measured time histories from those predicted. The residual PSDs were included as a third overlaid plot. An example is shown in log-log axes over the full frequency range for the 90° leg of rosette 12, **Figure 21**. The same PSD is also plotted on linear axes over the narrower frequency range of 0 - 30 Hz (**Figure 22**).

The results indicate that the predicted and measured strain PSDs are similar at frequencies < 40 Hz. At frequencies > 40 Hz the predicted strains are significantly over predicted.

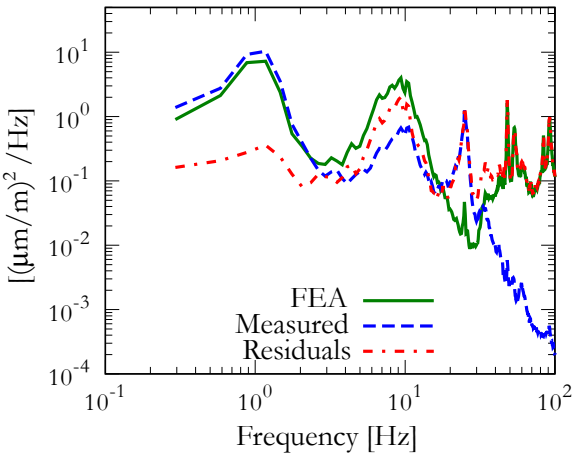

Figure 21: Comparison between Predicted and Measured Strain Time Histories, Converted into PSDs, Log-Log Scale, Full Bandwidth

To verify these results autocorrelation functions have been used. The autocorrelation function (ACF) calculates the correlation coefficient, ρ, of the signal by continuously shifting the signal relative to itself to build a plot of ρ vs lag, called the correlogram. An ACF has been calculated for

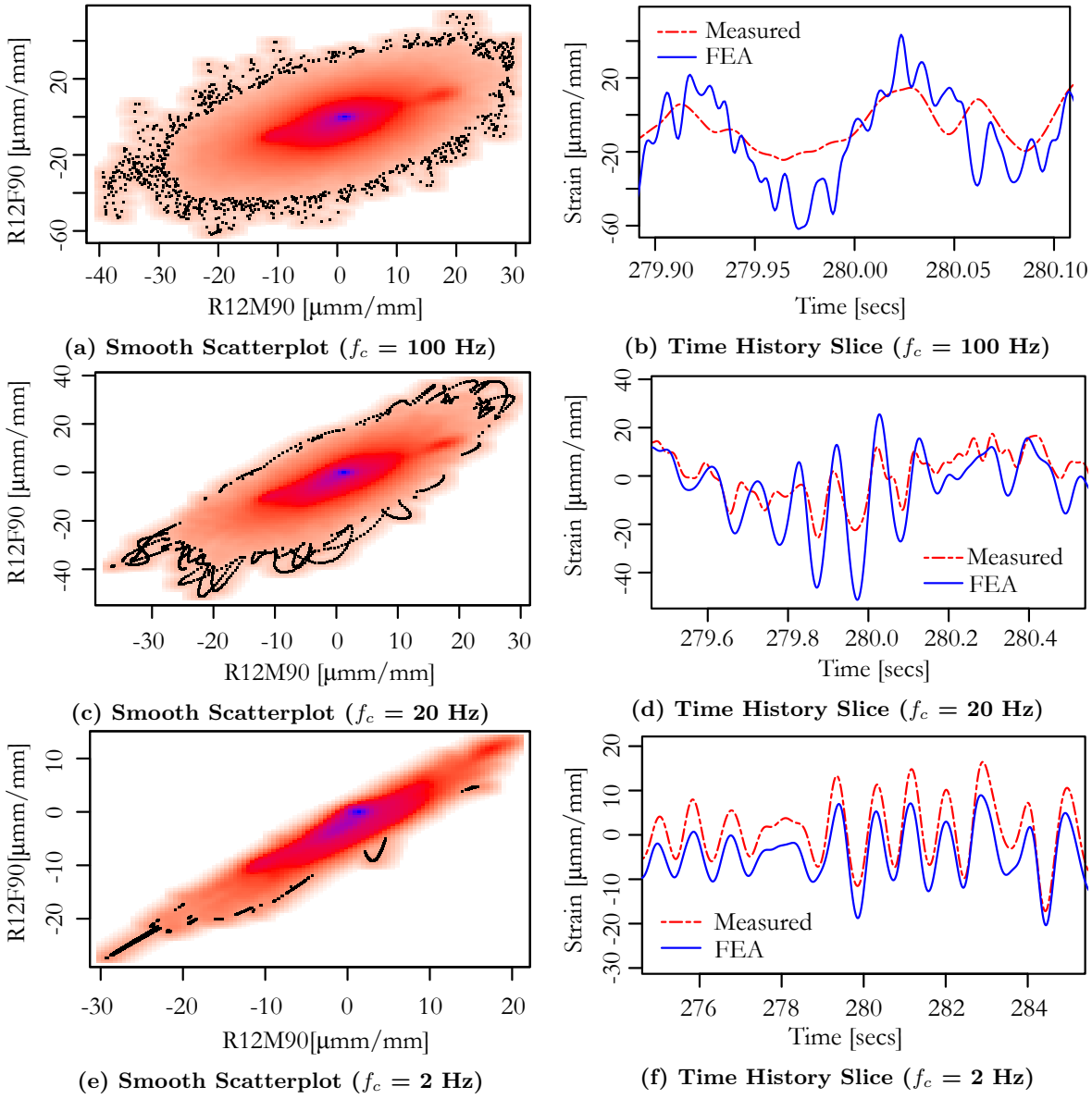

(a) Smooth Scatterplot (f_c = 100 Hz)

(b) Time History Slice (f_c = 100 Hz)

(c) Smooth Scatterplot (f_c = 20 Hz)

(d) Time History Slice (f_c = 20 Hz)

(e) Smooth Scatterplot (f_c = 2 Hz)

(f) Time History Slice (f_c = 2 Hz)

Figure 20: Effects of (f_c) on Correlation of Strain Gauge Rosette 12

each correlated, measured strain signal and also for each residual time history.

Figures 23 & 24 show correlograms from the measured strains of the 90° leg of rosette 12 and the residuals. The correlogram of the measurements possesses a narrow band signature, which is due to the peak between 0 - 3.5 Hz. The residuals on the other hand tend towards a white noise signature, demonstrating that the model succuessfully predicts the dominant trend in the measured strains.

Discussion

Data for fatigue load cases are currently in shortage for tie down design. This is due to the wide variation of packages and transport systems, difficulties in collecting experimental data and limited usage schedules. The type of data presented here is ideal for fatigue assessments, but larger measured strains would be necessary to calculate fatigue life and perform comparative fatigue analysis. A rainflow cycle count of the acceleration signals would produce conservative data for fatigue load cases by selecting a low pass filter cutoff frequency > 3.5 Hz.

A dynamic model would be more suitable for predicting response > 3.5 Hz. The results of this study have shown that the small strains at higher frequencies are unlikely to cause fatigue damage and therefore no attempt to produce a dynamic model has been made.

Examining the lower frequency range more

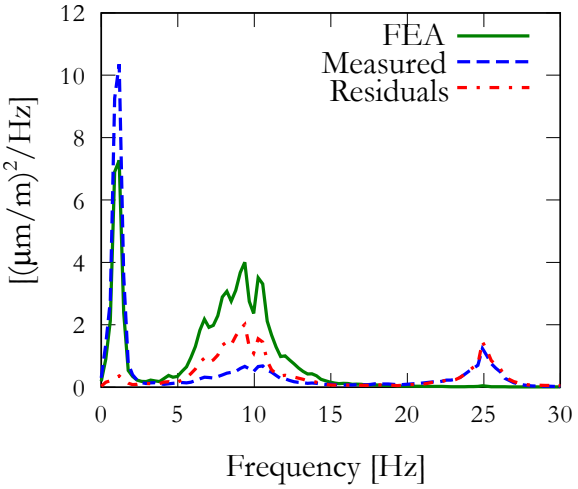

Figure 22: Comparison between Predicted and Measured Strain Time Histories, Converted into PSDs, 0 - 25 Hz

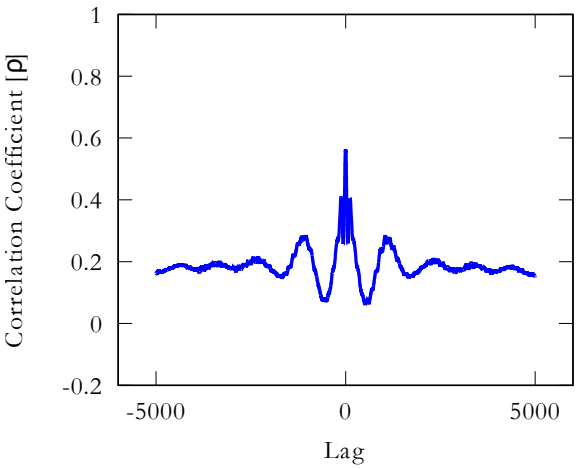

Figure 23: Correlogram of the Measured Strain Signal from the 90° Leg of Rosette 12

closely it is clear that the agreement between 0 - 3.5 Hz is very good. In the range 3.5 Hz - 15 Hz the predicted energy content in the strain signals is higher than in the measured signals. This concurs with expectations; a linear static model is only really suited to predicting very low frequencies.

To improve agreement the linear scaling and superposition procedure could be adapted to handle contact nonlinearities. One method to achieve this is to fit polynomial response functions of finite element stresses at each rosette location, based on a set of nonlinear analysis results that consider the measured load ranges and various combinations of loading. The scaling can than proceed by calculation of the strain time histories based on the fitted polynomials.

The analysis showed that the mean square of

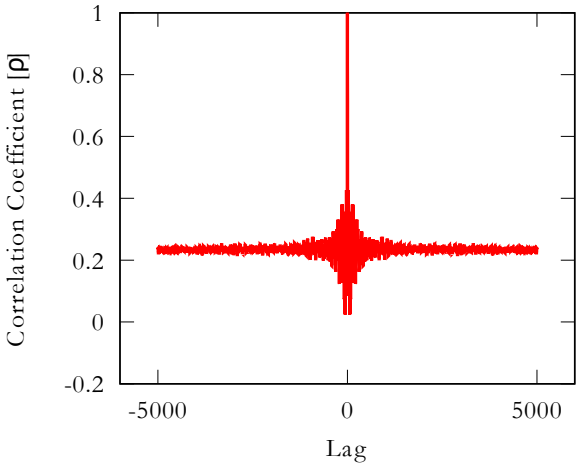

Figure 24: Correlogram of the Residuals between the Measured and Predicted Strain Signal from the 90° Leg of Rosette 12

the signals were often underpredicted at very low frequencies, possibly as a result of the chosen finite element discretization size. However at frequencies greater than 3.5 Hz treating measured accelerations as quasi-static tends to overpredict the spectral content and therefore the fatigue damage and peaks. This is attributed to the large inertia of the package which attenuates any high frequency strain response.

At higher frequencies the acceleration response measured nearest the package is also attenuated, this model demonstrates that a linear relationship between measured accelerations and strains does not exist at higher frequencies, i.e. the linear model tends to overpredict higher frequencies strains because it does not include inertial dynamic effects.

Conclusions

- A linear static FEM of a tie down system of a 99.7 tonne nuclear package has been successfully validated using strain and acceleration measurements with weak signal content.
- It was demonstrated that at least moderate correlation can be achieved with a properly prepared, linear static FEM.
- Spectral and residual analysis highlighted that the dominant source of loading occurred as a narrow band process between 0 - 3.5 Hz and the FEM correlation was strong at these frequencies.
- This level of agreement between FEA and a field experiment, which is highly uncontrollable, is very satisfactory.

References

[1] A. D. Cummings, J. Krywonos, P. Purcell, G. Rothwell, and C. Matthews. "Filtering and Analysis of Accelerations and Strains Measured on a Tie Down System of a Heavy Nuclear Transport Package during a Routine Rail Journey". *Packaging, Transport, Storage & Security of Radioactive Material*, 24(1):23–35, March 2013.

[2] Paul H. Wirsching, Thomas L. Paez, and Keith Ortiz. *"Random Vibrations: Theory and Practice"*. Dover Publications Inc., Mineola, NY, June 2006.

[3] Julius S. Bendat and Allan G. Piersol. *"Random Data: Analysis and Measurement Procedures"*. Wiley-Blackwell, 4th edition edition edition, March 2010.

[4] *BS EN 15433-3:2007 "Transportation Loads - Measurements and Evaluation of Dynamic Mechanical Loads - Part 3: Data Validity Check and Data Editing for Evaluation"*. BSI Standards Limited, 2007.

[5] Altair. Hyperworks 12.0.

[6] Dessault Systemes. Abaqus 6.13.

[7] *BS EN 10025-6:2004 "Hot rolled products of structural steels Technical Delivery Conditions for Flat Products of High Strength Structural Steels in Quenched and Tempered Condition"*. BSI Standards Limited, 2004.

[8] James Carvill. *"Mechanical Engineers Data Handbook"*. Butterworth-Heinemann, December 2012.

[9] *BS EN ISO 898-1:2013 "Mechanical Properties of Fasteners made of Carbon Steel"*. BSI Standards Limited, 2013.

[10] Yung-Li Lee. *"Metal Fatigue Analysis Handbook: Practical Problem-solving Techniques for Computer-aided Engineering"*. Butterworth-Heinemann, August 2011.

[11] Peter Heyes, John Dakin, and Christopher St.John. The Assessment and Use of Linear Static FE Stress Analyses for Durability Calculations. In *9th International Conference on Vehicle Strutural Mechanics and CAE*, Warrendale, PA, April 1995. SAE International.

[12] HBM nCode. Design Life 9.1.

[13] Michael Speckert. "Calculation of Stress Time Signals of Multi Bolted Joints Located at a Ball Joint of a Railway Vehicle". Technical report, Idealisation of Bolted Joints, NAFEMS, 2010.

[14] R Core Team. "R: A Language and Environment for Statistical Computing. R Foundation for Statistical Computing", 2014.

[15] John W. Eaton, David Bateman, and Soren Hauberg. *GNU Octave version 3.0.1 manual: a high-level interactive language for numerical computations*. CreateSpace Independent Publishing Platform, 2009. ISBN 1441413006.